1 **Ice buttressing-controlled rock slope failure on a cirque headwall,**

2 **English Lake District**

4 Paul A. Carling[a, b,] John D. Jansen[c], Teng Su[d, e], Jane Lund Andersen[f], Mads Faurschou

5 Knudsen[f]

6 [a] Geography and Environmental Science, University of Southampton, Southampton, SO17

7 1BJ, UK.

8 [b] Lancaster Environment Centre, Lancaster University, Bailrigg, Lancaster, LA1 4YW, UK.

9 [c] GFÚ Institute of Geophysics, Czech Academy of Sciences, Prague, Czechia.

10 [d] University of Chinese Academy of Sciences, Beijing 100049, China.

11 [e] Laboratory of Water Cycle and Related Land Surface Processes, Institute of Geographical

12 Sciences and Natural Resources Research, Chinese Academy of Sciences, Beijing, 100101,

13 China.

14 [f] Department of Geoscience, Aarhus University, Aarhus, Denmark.

16 Corresponding author: Paul A. Carling (p.a.carling@soton.ac.uk)

18 **Key Points**

19 Geometry and mechanics of cirque rock slope failure defined from the local geology

20 Rock slope failed slowly due to ice buttressing the cirque headwall

21 Rock slope failure occurred during deglaciation

Abstract

Rock slope failures in the English Lake District have been associated with deglacial processes after the Last Glacial Maximum, but controls and timing of failures remain poorly known. A cirque headwall failure was investigated to determine failure mechanisms and timing. The translated wedge of rock is thin and lies on a steep failure plane, yet the friable strata were not disrupted by downslope movement. Fault lines and a failure surface, defining the wedge, were used as input to a numerical model of rock wedge stability. Various failure scenarios indicated that the slope was unstable and would have failed catastrophically, if not supported by glacial ice in the base of the cirque. The amount of ice required to buttress the slope is insubstantial, indicating likely failure during thinning of the cirque glacier. We propose that, as the ice thinned, the wedge was lowered slowly down the cirque headwall gradually exposing the failure plane. A cosmogenic ^{10}Be surface exposure age of 18.0 ± 1.2 ka from the outer surface of the wedge indicates Late Devensian de-icing of the back wall of the cirque, with a second exposure age from the upper portion of the failure plane yielding 12.0 ± 0.8 ka. The 18.0 ± 1.2 ka date is consistent with a small buttressing ice mass being present in the cirque at the time of regional deglaciation. The exposure age of 12.0 ± 0.8 ka represents a minimum age, as the highly-fractured surface of the failure plane has experienced post-failure mass-wasting. Considering the chronology, it appears unlikely that the cirque was re-occupied by a substantial ice mass during the Younger Dryas Stadial.

Key words:

rock slope failure, Pleistocene glacial cirque, cosmogenic exposure dating, deglaciation, Younger Dryas, English Lake District.

1   Introduction

There are at least 84 known or suspected rock slope failures (RSFs) in the Lake District of NW England that have been associated with the Late Devensian glaciation (Marine Isotope Stage 2: Wilson *et al*., 2004; Jarman and Wilson, 2015a; Wilson & Jarman, 2022). Such RSFs often are termed 'paraglacial' as they "are part of, or influenced by, the transition from glacial conditions to non-glacial conditions" (Ballantyne, 2002; McColl, 2012). However, the relationship between glaciation, deglaciation, and the occurrence of RSFs remains far from resolved. This paper provides a contribution to further understanding of the topic. While a

few highly modified landforms have been identified tentatively as RSFs and related to time periods before the Last Glacial Maximum (LGM; c., 26.5 ka BP to 19 ka BP, Clark et al., 2009) (Jarman and Wilson, 2015b), the majority of Lake District RSFs have been associated with the end of the Dimlington Stadial (see 'Glacial Context') and the final down-wasting of the Late Devensian ice sheet within NW England. At that time, potential RSFs could have been fully supported or partially supported by residual ice masses in topographic lows. Alternatively, some RSFs could have occurred (Wilson, 2005) following the Scottish Readvance (*c.*, 19.3 – 18.2 ka; Chiverrell *et al.*, 2018) and the Younger Dryas Stadial (12.9 – 11.2 ka; Rasmussen *et al.*, 2006). However, only one disintegrated RSF has been dated. In contrast, those that represent steep-slope deformation, or arrested slides, are of unknown age (Jarman and Wilson, 2015b). An arrested hillslope failure occurs when the slipped mass is not evacuated from the source area (Jarman, 2005), but is retained on the slope of the footwall. The role of glacial ice in buttressing rock slopes, and thereby preventing failure (Whalley *et al.*, 1983; Holm *et al.*, 2004; Cossart *et al.*, 2008; Le Roux *et al.*, 2009; Allen *et al.*, 2010; Hilger *et al.*, 2018), is largely speculative (Ballantyne, 2002; Jarman and Wilson, 2015b; Cody *et al.*, 2018; Hartmeyer *et al.*, 2020) and controversial (McColl *et al.*, 2010), as are the mechanics of slope failure in situations where ice-support progressively diminishes (McColl and Davies, 2013; Klimeŝ *et al.,* 2021; Cave and Ballantyne, 2016). The latter two generic issues are the primary focus of this paper.

Glacial erosion can steepen cirque headwalls to the extent that faulted and/or fractured-rock slopes become unstable (Sass, 2005; Moore *et al.*, 2009), if not ice-supported. In addition, the way slopes fail can provide insight to whether ice was present during the slope failure. If ice-buttressed failures can be dated, then RSFs provide a source of information on the timing of the final ice retreat. Here, an arrested (*sensu* Jarman, 2005) translational RSF is described, dated, and the likely controls on the failure are defined and modelled. We test the hypothesis that *a steep, faulted, and unstable rock slope has experienced buttressing by glacial ice*. Our study area, which has not been previously identified as a RSF site, is within Great Coum (54.3923° N, 2.6057° W), a small cirque within the southern Shap Fells to the west of the Lune gorge (Fig. 1). A neighbouring cirque is named Little Coum. The Lune gorge (south of Tebay; Fig. 2) separates the southerly extension of the Shap Fells to the west from the Howgill Fells to the east. The site details and glacial context are described below.
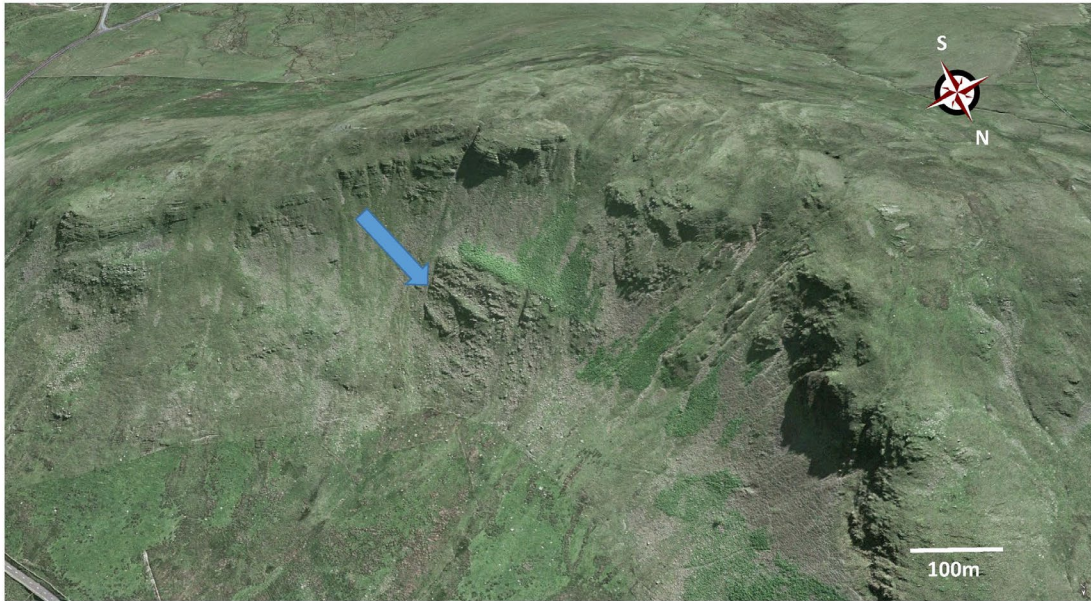
Fig. 1: Oblique aerial view, looking southwestward, into Great Coum (Google Earth image). The RSF is arrowed. The green grassy tread of the RSF (just above the arrow) is in sunlight below the cliffed headwall (in shadow). The breadth of the RSF is between 125m and 180m. Little Coum is just out of view to the right. Base image © Google Earth 2014. Scale bar applies to the middle distance.
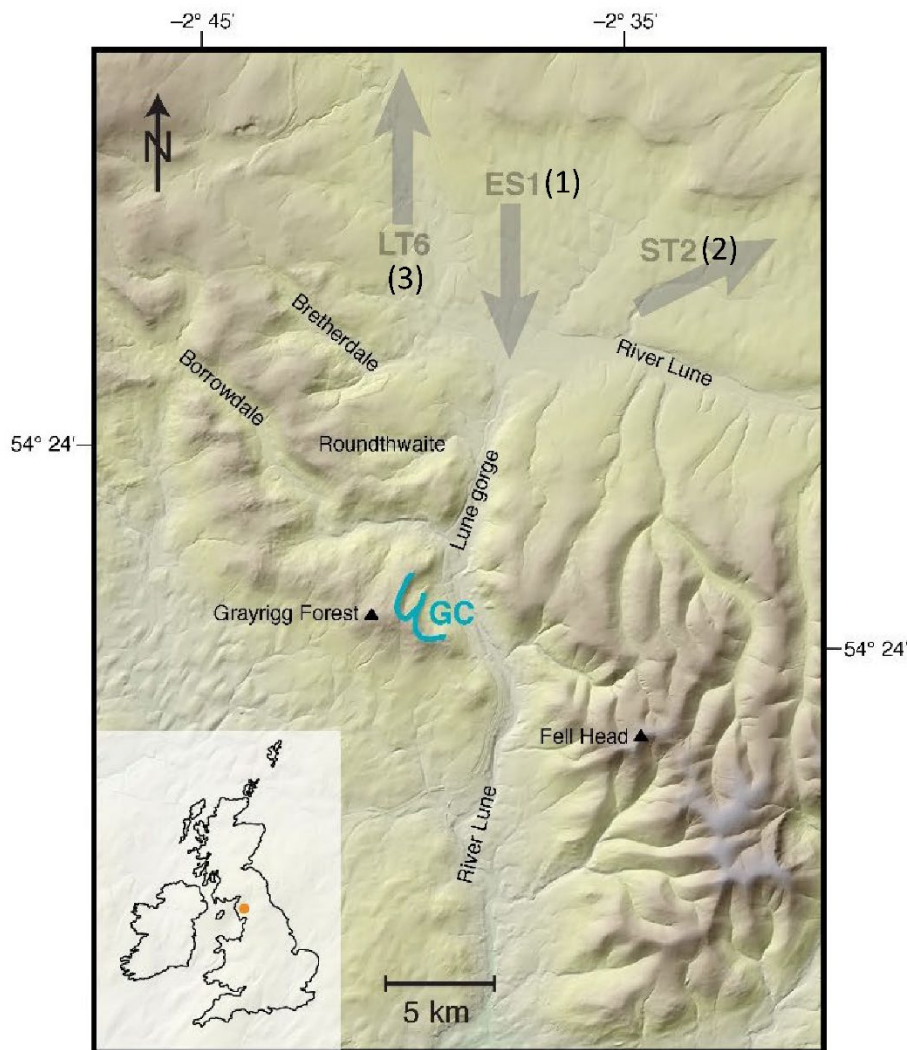
96

97

98 Figure 2: Regional map showing the location of Great Coum (GC) and Little Coum with
99 respect to generalized Dimlington (ES1), (ST2) and (LT6) ice movements (after Livingstone et
100 al., 2010; 2012). Labels (1), (2) and (3) indicate the temporal sequence of ice movements.
101 Locations referred to in the main text are also shown. Inset shows the location of the study
102 area in the context of the British Isles. Base NEXTMap digital elevation topography has a 5 m
103 resolution.
104

105 **2   Glacial Context**

106 The last period of extensive glaciation in northern Britain occurred during the Dimlington

107 Stadial of the Late Devensian substage of the Pleistocene (~28-15 ka; Rose, 1985; Scourse *et*

108 *al*., 2009; Chiverrell and Thomas, 2010; Davies *et al*., 2019), equivalent to Stadials 3 and 2 of

109 the North Greenland Ice Core Project (NGRIP) chronology (Lowe *et al*., 2008) and the Marine

110 Isotope Stage 2 (Ehlers and Gibbard, 2013). During the LGM, the Lune gorge and surrounds

111 were covered by several hundred metres of ice. The Lune gorge is ice-sculpted, having a

112   parabolic bedrock cross-section with truncated valley-side spurs along both the west and the

113   east margins. Great Coum and Little Coum, on the western side of the gorge, are the only

114   recognized cirques in the Lune gorge. These two Lunedale cirques should not be confused

115   with two cirques with the same names in Dentdale (Barr *et al.*, 2017). The two conjoined

116   embayments were considered by Marr and Fearnsides (1909) to be a single cirque, but

117   recently have been recorded as separate cirques (Barr *et al.*, 2017; Clark *et al.*, 2018).

118   Devensian till banks and moraine (entrenched by the River Lune) fill much of the Lune gorge

119   floor and till also occurs in most tributary valleys (Aveline *et al.*, 1888; Marr and Fearnsides,

120   1909; BGS, undated; 2008 a and b).

121

122   **2.1   Complexity of Devensian glaciation around Great Coum**

123

124   The context in which the RSF occurred is relevant to the interpretation of the importance of

125   potential ice buttressing and is referred to within the Discussion. Here we provide the

126   setting. Little is known of the glacial history of the Lune gorge area (Carling *et al.*, 2023).

127   Nevertheless, prior findings, in the main, have been incorporated in the BRITICE maps of the

128   area (Stokes *et al.*, 2018). A complex interplay occurred in the vicinity of the Lune gorge

129   between several upland ice dispersal centres, primarily: the Scottish, Lake District and

130   Howgill ice masses, during the period of maximum ice cover ~ 26–22 ka. All three ice masses

131   interacted in the north whilst the latter two ice masses dominated to the south. After the

132   LGM, as the ice sheets down-wasted and ice flows became increasingly valley-confined, ice

133   emanating from the two cirques would have flowed northwards (Carling *et al.*, 2023).

134

135   The complexity of regional ice flow was simplified by Livingstone *et al.* (2010; 2012) by using

136   codes to refer to different ice streams (Fig. 2) that occurred in various locations and at

137   differing times; the relevant codes are as follows. In the ES1 phase, early LGM, northern ice

138   penetrated a short distance into the Lune gorge (Harkness, 1870; Goodchild, 1875; 1889;

139   Marr and Fearnside, 1909; Hollingworth, 1931; Moulson, 1966; Letzer, 1978) as far as

140   Carlingill and Great Coum (Fig. 2) but no further. However, Davies *et al.* (2019)

141   demonstrated that, close to the LGM, (ST2 phase; *sensu* Livingstone *et al.*, 2010) and during

142   the LT6 phase (Chiverrell *et al.*, 2018), ice flowed northwards from the Lune gorge (Fig. 2).

143   On the northern flank of the Howgill Fells, any ST2/LT6 ice flow would have been to the

144   north and east from the Howgill ice dome (Fig. 2) such that the higher summits of the

145   Howgill Fells were not overrun by ice from further north (Gunson, 1966; Stone *et al.*, 2010).

146   Rather, the Howgill Fells hosted its own local ice dispersal centre. Prior work failed to

147   determine whether northern ice entered the two Lunedale cirques. Consistent northerly

148   down-wasting ice-flow was established (Hollinsworth, 1931; Rose and Letzer, 1977) from 19

149   ka (Davies *et al.*, 2019) with surrounding areas north and south of the Lune gorge being ice

150   free by ~ 19.2 to 16.6 ka (see Carling *et al.*, 2023, for a review of regional dates). These dates

151   are broadly consistent with other dates for deglaciation of the central Lake District more

152   widely (Wilson and Lord, 2014) and are indicative of a general ~ 2–3 kyr window for the

153   timing of final Dimlington ice down-wasting within the Lune gorge when the back wall of the

154   Great Coum cirque could have become ice-free. We return to this point in sections 3 and

155   6.2.

156

157   Given that ice may have reoccupied upland terrain in Lake District during the Younger Dryas

158   (Brown *et al.*, 2013; Bickerdike *et al.*, 2018), in principle, an ice mass may also have occurred

159   in the general vicinity of the Lunedale cirques at this time. However, no evidence for

160   Younger Dryas ice in the Lune gorge has been reported.

161

162   **3   Geological Setting of the cirques**

163

164   The bedrock in the cirques comprises the marine Silurian Coniston Group (Soper, 1999;

165   Soper, 2006), which here consists of fine-grained, blue-grey, sandy siltstone (greywacke) and

166   sandstones in beds from < 1 m to ~ 3 m thick. Most of the thicker beds crop-out within the

167   headwalls of the cirques. The thicker sandstone beds are more competent with fewer

168   fractures, whilst thinner fissile siltstone beds exhibit cleavage and are heavily fractured.

169   Vertical joints are frequent with spacings of a few metres, together with evidence of small-

170   scale bedding deformation and small-scale faulting. Moseley (1968; 1972) considered the

171   considerable complexity of the regional structure and noted folding, steep discontinuous

172   local faulting, joint patterns and the presence of slickenside surfaces in the southern Shap

173   Fells. In the Methods and the Results, this complexity is not considered, as the detail is not

174   pertinent to our study. None-the-less, reference is made to local steep faults, slickenside

175   surfaces and friability where these are relevant, as the rock structure in the vicinity of the

176 RSF is critical in assessment of slope stability (Bonilla-Sierra *et al.*, 2015; Stead and Wolter,

177 2015). The apparent dips of the local beds range from 0º to 30º, SW into the headwall of

178 Great Coum. However, the apparent 8º plunge of the stratal sequence is towards the NW,

179 such that the true dip is to the WSW with a NW strike (BGS, 2008 a and b). Infrequent, but

180 distinctive 10– 40 mm-thick pale bands of siltstone occur (*e.g.,* Taylor *et al.,* 1971, p. 26) in

181 some of the thicker beds, which extend discontinuously over distances of several

182 decametres parallel to the primary bedding. These siltstone bands are significant in that

183 examples (here termed marker horizons) occur in the headwall strata which correlate with

184 similar siltstone bands in the strata of the RSF.

185

186 Great Coum is orientated NE, Little Coum is orientated NNE. The orientations of the cirques

187 are influenced by the strike of local paired anticlines (Marr and Fearnside, 1909; BGS,

188 2008a), and the low-insolation aspects of both sites would have encouraged Devensian snow

189 and ice accumulation and preservation. Great Coum exhibits no distinct lip (i.e., no

190 overdeepening), the ground falls steadily from around 237 m (height above mean sea level,

191 m asl) to the River Lune below (Fig. 3A). Above 300 m the ground rises more steeply to

192 rocky head walls locally near 80º at 360–440 m, giving a height range of around 225 m. Little

193 Coum exhibits a slight lip at around 262 m altitude. Above 400 m the ground rises more

194 steeply to near 80º rocky head walls at 400–440 m, and the ridge crest at 480 m gives a

195 height range of around 220 m (Fig. 3B). First to second-order minor streamlets occupy the

196 lower parts of Great Coum, and Little Coum is drained by the third-order stream, Burnes Gill.

197

198

199

200
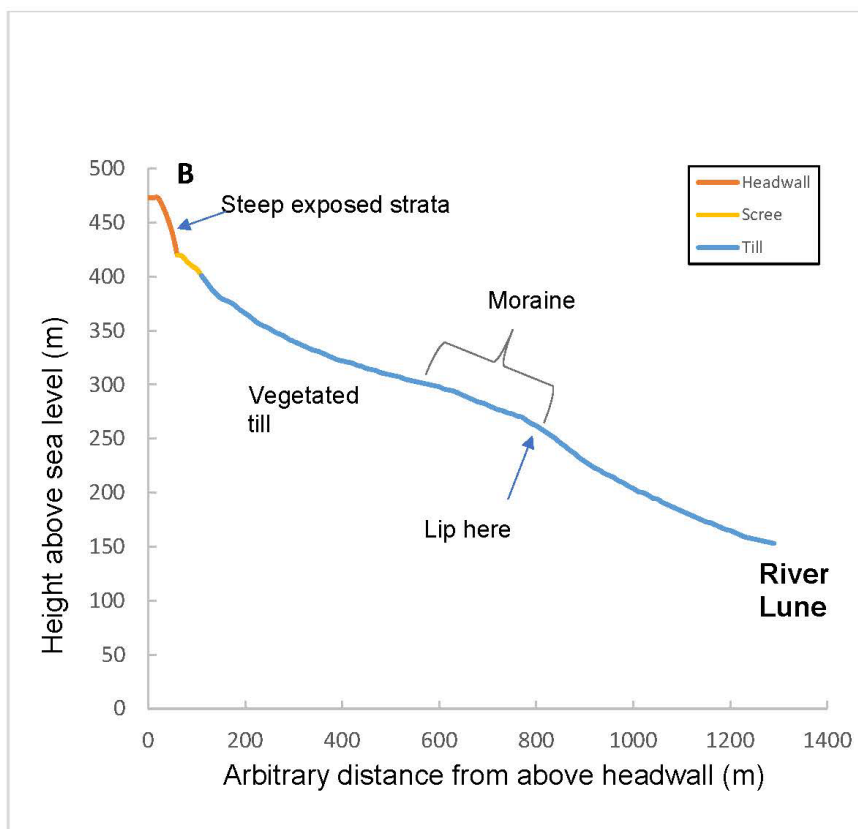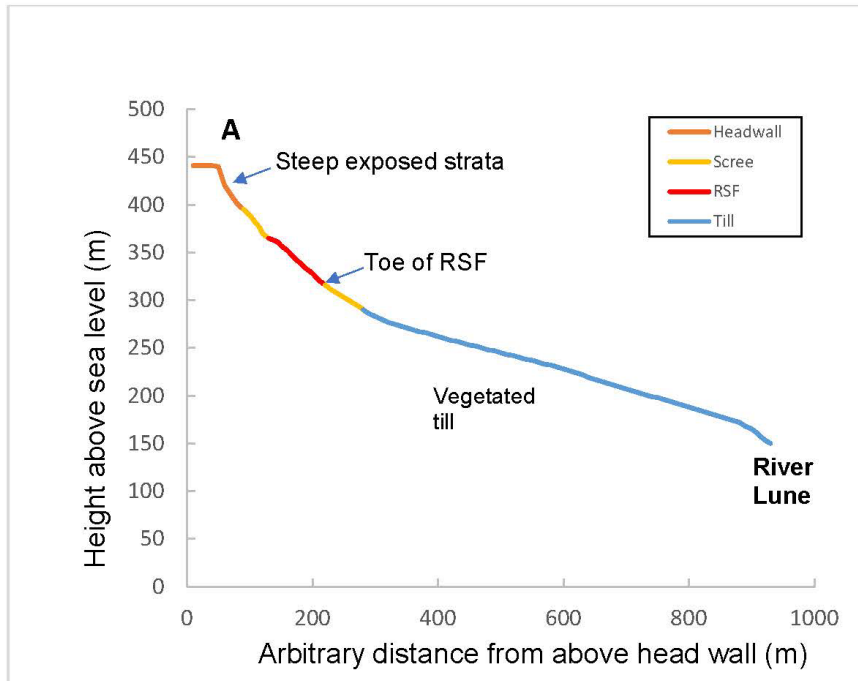
201

202 Figure 3: Long profiles along centre of cirque: (A) Great Coum; transect from 54.389978 N;
203 2.606625 W to 54.396675 N; 2.598278 W; (B) Little Coum; transect from 54.393789 N;
204 2.615992 W to 54.400117 N; 2.602208 W. Exposed bedrock is indicated in the headwall and
205 in the RSF. Data extracted from Google Earth.
206

207   The British Geological Survey (BGS,2008b) map identifies till on the lower slopes of Great

208   Coum and the BGS borehole database contains the records of 24 shallow boreholes ranged

209   along the axis of the Lune gorge over 1.25 km immediately below Great Coum. These

210   borehole logs show that the slopes just below the cirque consist of a thin soil above a 2.5 m

211   thickness of Devensian diamicton, overlying the Silurian Coniston Grit. In Little Coum,

212   hummocky till infills the cirque below 400 m (BGS, 2008b); at lower altitudes, a flatter thin

213   diamicton drapes much of the basin, including a poorly defined curvilinear moraine that

214   terminates at the lip (Fig. 3B). It is not possible to calculate an equilibrium line altitude (ELA)

215   with any certainty based on the upper limit to highest lateral limits to the curvilinear

216   moraine (Porter, 2001), but 300 m asl is a reasonable estimate. Bedrock exposures along

217   Burnes Gill and augering during the current project indicate that this moraine is no more

218   than 6 m thick. The curvilinear moraine has a distinctive, sharp, outer margin along the

219   rocky rounded ridge that separates the two cirques. Within Little Coum, three faint

220   diamicton-covered (possibly ice-recessional) benches occur on the northern slope of the

221   cirque. Thus, although Great Coum lacks any preserved indication of ice retreat, such

222   indicators may exist within Little Coum.

223

224   All the deposits described above are significant. In the first instance, substantial till in the

225   Lune gorge below Great Coum has been related to northern ice penetrating the gorge

226   around the LGM (Carling, *et al.*, 2023). At that time, the whole region was covered by a thick

227   ice sheet (Merritt *et al.*, 2019). However, as down-wasting led to increasing topographic

228   control and valley glaciers predominated, there was likely to be ice flow out of the cirques

229   prior to the near-complete ice retreat that left the diamicton-covered benches. We envisage

230   that around the LGM, thick overriding ice in the vicinity of Great Coum was dictated by

231   regional ice gradients largely independent of the local topography (Carling *et al.*, 2023).

232   Post-LGM, ice-discharge from the cirque initially would have remained high but any

233   buttressing effect on the headwall would decline as the ice thinned.

234

235   The RSF occurred in Great Coum. The most southerly backwall section of the cirque consists

236   of a steep rocky headwall facing N, whilst to the west a further steep rocky headwall faces

237   NE; a steep grassy slope occurs between these two outcrops. The RSF caused headwall

238   retreat in the vicinity of the present grassy slope, leaving the intact steep rocky sections of

239   the backwall to either side, but the failure also extends below the north-facing headwall (Fig.

240   1). Indistinct, small RSFs also occur to the east and west, which are not considered further.

241   Little Coum also contains a steep rocky headwall, but with no evidence of slope failures. The

242   mass of the RSF in Great Coum appears to have descended as a translational near-intact

243   block. Although a near-vertical fracture occurs in the right-hand side of the slipped mass

244   (Fig. 4), in other respects the undisturbed strata within the block readily correlate with strata

245   in the headwall above.

246

247   **4   Materials and Methods**

248   **4.1   Mapping landscape features**

249   The British Geological Survey (BGS, 2008a) records several lineaments in the vicinity of

250   Great Coum that represent small faults or large block joints. Google Earth satellite images

251   (2004, 2009, 2011 and 2014) were used to visually identify these linear landscape features

252   as well as others of relevance (not recorded by the BGS). Lineaments trace topographic

253   discontinuities, stratigraphic offsets, vegetation differences and slickensides, and these

254   forms were checked in the field. Smaller-scale linear features consist of the silt banding

255   marker beds, and numerous minor joints (the latter not mapped). The various points of

256   interest were recorded as single point data in the field using a hand-held Garmin global

257   positioning system (GPS). The strikes of bedding and the direction of faults were recorded

258   as compass bearings whilst the dips of bedding and faults were recorded relative to a

259   horizontal plane using a digital clinometer.

260

261   Single point data are precise in planview whereas linear features, between two or more

262   well-determined points, provide the general trend of features such as gullies and faults.

263   GPS coordinates also were used to map the extent of the slumped block. Due to the

264   inaccuracy of hand-held GPS-derived altitudes, the planview GPS coordinates were used to

265   determine the altitude of each point from Google Earth, and these were taken as definitive

266   (error < 4%) after cross-checking with Ordnance Survey 1:50,000 maps (Harley, 1975).

267   Selected topographic profiles were also developed from Google Earth imagery by reading x,

268   y and z coordinates at 10m horizontal spacings along selected planview lines running from

269   the top of the headwall of each cirque, across the free face and the slope below. Finally, a

270   systematic search was made within both cirques for Shap granite or limestone erratics to

271   check whether northern ice had entered the cirques. Outcrops of both these lithologies

272   occur 10km to the north.
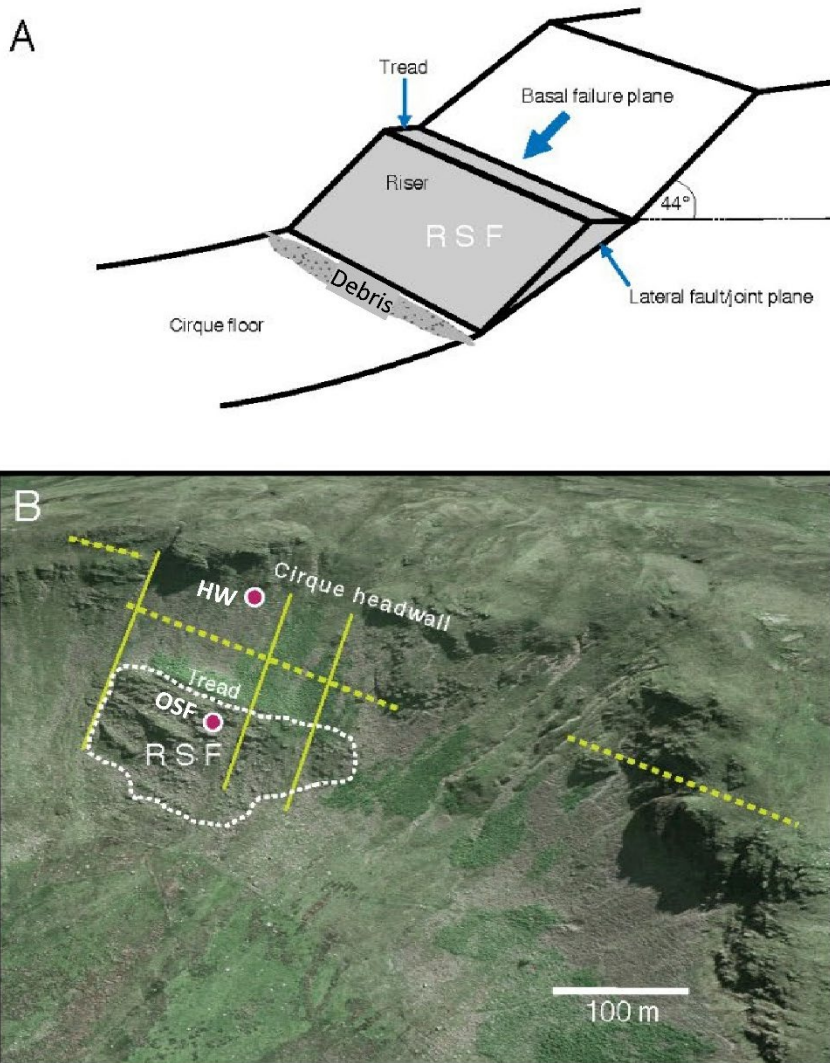
273

274

275

276   Figure 4: A) Schematic cartoon of a simple wedge failure to indicate the terminology used

277   within the main text. B) Annotated view of Great Coum (compare Fig. 1). The fault-aligned

278   rock slope failure plane (c), above and behind the RSF, is intersected by three major steep

279   fault lines, the outer two of which (X,Y) define the RSF model. The locations of samples (HW

280   and OSF) collected for exposure dating are shown by circled symbols. Base image © Google

281   Earth 2014. Scale bar applies to the middle distance.

282

283   We refer the reader to Figure 4A for an explanation of the RSF terminology used here,

284   although the failure planes bounding the wedge are omitted for clarity. The modern

285   headwall of the cirque locally constitutes the main exposed scarp of the failure plane behind

286   the translational wedge of the RSF. The outer face of the wedge is termed the 'riser' and the

287   near-horizontal head of the wedge is termed the 'tread'.

288

289   **4.2   Rock sampling for surface exposure dating**

290   Terrestrial cosmogenic radionuclides, such as [10]Be, are produced and accumulate in minerals

291   within a few metres of Earth's surface due to their exposure to secondary cosmic rays and

292   are lost via erosion and radionuclide decay (Lal, 1991). In our case, two free rock surfaces

293   are recognised (Fig. 4): the riser, being the outer surface of the RSF, and the tread, which

294   forms the top surface of the slipped mass. We set out to determine when the RSF riser was

295   first exposed to cosmic rays as ice receded from the cirque. For reasons of economy, we

296   collected one sample from the riser to compare the exposure age with the timing of

297   regional deglaciation. A ~15 kg intact block of bedrock (sample OSF) was collected from the

298   outer 10 cm-thick surface of the riser (Fig. 4B); a prominent thick undisrupted stratum close

299   to the top of the RSF mass, which was ice?-smoothed (Fig. S3). Our sampling strategy was

300   restricted by the ease of access and by the nature of the bedrock surfaces. The smooth

301   bedrock surface of the riser we sampled suggests minimal loss of rock mass due to surface

302   fragmentation or spalling since the RSF occurred. A second 15 kg bedrock block (sample

303   HW) was collected from the failure plane of the transverse fault line (Fig. S3) just below the

304   cirque headwall (Fig. 4B) with an aim to determine the timing of the failure. The sampled

305   bedrock failure plane was observed to be densely fractured, suggesting some loss of

306   material from the surface since its exposure. Surface erosion affects the abundance of

307   cosmogenic nuclides and the estimated exposure age; an issue we address in the Discussion

308   (and Supplementary Materials). Samples were cut from *in situ* bedrock surfaces using a

309   powered rock saw, their altitude, bearing, tilt, and topographic shielding were recorded.

310   Topographic shielding is significant for both samples; details are given in Fig. S1

311   (Supplementary Materials).

312

313   Our approach entails three important assumptions about the last glaciation. First, we

314   assume that the cirque headwall experienced at least 2 m of bedrock glacial erosion, which

315   removed the nuclide inventory produced during preceding ice-free periods; and second, that

316   ice burial depth at the position of the OSF sample was at least 20 m and therefore sufficient

to effectively halt nuclide production and third, that this cover persisted until failure. These

assumptions mean that sample OSF began accumulating ^{10}Be only from the time that the

down-wasting ice exposed the surface to cosmic rays. In contrast, sample HW remained

deeply shielded (> 5 m) within the cirque headwall until the RSF exposed the failure plane

to cosmic rays.

4.3   Cosmogenic nuclide analysis

The two bedrock samples were prepared for cosmogenic ^{10}Be analysis at the Aarhus

University Cosmogenic Nuclide Laboratory, Aarhus, Denmark, following standard laboratory

procedures as described in Andersen *et al*. (2020). The ^{10}Be/^{9}Be ratios were analysed at the

accelerator mass spectrometer at AARAMS, Aarhus, Denmark. A summary of the

cosmogenic nuclide analyses is given in Table 1 and further details are found within

Supplementary Materials.

Table 1. Summary of the cosmogenic nuclide analyses. ^{10}Be concentrations in quartz
normalized to the "07KNSTD" standardization by Nishiizumi *et al*. (2007), and exposure ages
calculated using LSDn scaling (Lifton *et al*., 2014) and global calibration dataset (Borchers *et al*., 2016) via http://hess.ess.washington.edu v3.0.2. The analytical uncertainty includes AMS
error on measured ratios incl. standard uncertainty of 1.1. %, Be carrier concentration, and
processing blank propagation (<1.2 %). The total uncertainty also includes production scaling
and calibration uncertainties. Rock density was assumed as 2.7 g cm^3.

Sample ID	Latitude	Longitude	Elevation	Topo shielding correction	Sample thickness	^{10}Be	Uncert	^{10}Be age	Analytic uncert	Total uncert
			(m.a.s.l.)		(cm)	(at g^{-1})	(at g^{-1})	(ka)	(kyr)	(kyr)
HW	54.3907	–2.6065	415	0.74	1	57499	1975	12.0	0.4	0.8
OSF	54.3917	–2.6064	348	0.58	1	63969	2017	18.0	0.6	1.2

4.4   Rock slope failure modelling

The RSF was modelled using *Swedge* version 6.0 (2018), a specialised rock-slope stability

software package, which can analyse a five-sided block (pentahedron) as a translational

wedge-failure—whereby a rock mass slides along a persistent basal plane of failure

bounded on each side by a fault or joint plane (Hoek and Bray, 1981; Rocscience Inc., 2018).

Either, or both, laterally bounding faults can act as additional slide planes, depending on

346 the geometry of the problem (Fig. 4A). In our case, two surfaces are not confined by

347 neighbouring bedrock: the outer surface of the RSF, the riser, and the top surface of the

348 slipped mass, the tread (Fig. 4). As well as varying the geometry of the failure and the

349 roughness of the failure planes, *Swedge* has options to consider the influence of: (i) a

350 tension crack at the back of the failure (not shown in Fig. 4A); (ii) water in the failure planes;

351 and (iii) the effect of any restraining normal stress that may counter the propensity to slide.

352 In engineering applications, restraining normal stress is conventionally realized using steel

353 rock bolts, or stone and concrete structures applied to the face of the riser, especially near

354 the toe. In contrast, here the issue is whether an ice mass in the cirque can buttress a slope

355 that is otherwise unstable, as is explored below. In glaciated mountain environments,

356 permafrost (and ice segregation) can penetrate bedrock to a depth of several metres

357 (Andersen *et al*., 2015). Ice-filled fissures tend to be stable at temperatures below –2°C,

358 which gives rise to the concept of 'ice-cemented' fractures (Ballantyne, 2018).

359 Consequently, the possibility that permafrost stabilized the RSF failure planes is considered

360 in section 5.3.

361

362 *Swedge* was implemented adopting the Mohr-Coulomb failure criterion (*e.g.,* Jaeger and

363 Cook, 1979) pertaining to the limit equilibrium stability of a three-dimensional rock mass

364 using field data (Table 2). Further details are provided in the Supplementary Materials and

365 within the Results. Stability is defined in terms of a factor of safety (*F*) where *F* > 1 indicates

366 a stable slope and *F* < 1, a failed slope. *F* = 1 represents a critical state. In general terms,

367 the factor of safety is defined as the ratio of the forces resisting motion to the driving forces.

368 Driving forces include the mass of the wedge accelerated through gravity and water

369 pressure; the latter applied normal to each wetted plane. Resisting forces arise from the

370 shear strength of the wedge sliding planes. Any ice load on the wedge is considered only as

371 a weight force contribution to the normal stress. Thus, active support due to the load of any

372 glacial ice (or firn) on the riser is included in the analysis as in Equation 1; where T_n is the

373 normal component and T_s is the shear component of the force applied to the riser. Active

374 support is assumed to act in such a manner as to decrease the driving force in the factor of

375 safety calculation:

376

377 $$F = \frac{resisting\ force + T_n\ \tan\phi}{driving\ force - T_s} \qquad (1)$$

378

379 Unless parameter values are known exactly, a single deterministic RSF model cannot be

380 resolved using Equation 1. In view of the uncertainty, in our field case, related to the exact

381 relationship between fault plane alignments and dips, a variety of potential failure

382

Table 2. Parameter values for RSF as determined in the field and as explored within the three model scenarios.

	Riser Angle °	Tread Angle °	Riser length (m)	Riser Bearing °	Width of tread (m)	Breadth of RSF (m)	Failure Plane Dip °	Failure Plane Bearing	Failed volume (m³)	Fault X Dip orientation °N	Fault Y Dip orientation °N	Fault X bearing °N	Fault Y Bearing °N	Fault X Dip °	Fault Y Dip °	Tension crack
Field	53	1	70	24	15	179	44	11	Est: 68288	291	298	21	28	unknown	unknown	unknown
Model 1	53	1	75	24	15	182	44	24	68333	201	208	21	28	80	72	none
Model 2	53	1	75	24	15	182	44	24	67792	90	90	21	28	71	71	none
Model 3	53	1	110	17	15	125	44	11-14	68739	111	62	21	28	90	62	present

383

384 scenarios must be considered. To narrow the number of models, we used preliminary trials

385 of our field-derived parameter values as input, varying both strength and slope and

386 geometry parameters. Then, consideration of a range of fault plane dips allowed us to

387 exclude geometrically impossible configurations and those geometries that did not

388 resemble the geometry of the RSF. In this manner, we devised three model scenarios that

389 represent the RSF in terms of shape and mass. More than 10,000 simulations were

390 performed for each scenario, varying parameter values systematically (typically ± 10%) to

391 isolate the most probable model for each case. The uncertainty and probability analyses

392 were conducted using the dedicated approaches built into the *Swedge* platform, selecting

393 normal distributions to describe the possible range of parameter values; for example, ± 10°

394 of dips measured in the field. Finally, the buttressing effect of any glacial ice against the

395 potential RSF is considered by applying an external load evenly across the area of the riser

396 to counter any propensity for failure.

397

398 **5.0   Results**

399 **5.1   The rock slope failure**

400 The positions of the pale silt marker beds, located in the headwall and within the RSF,

401 indicate the RSF has moved downslope by about 110 m (*H*) vertically and up to 192m (*L*)

402   horizontally. The width of the tread is about 15 m; the breadth of the slide is between 125

403   and 180 m and the vertical extent of the main slipped intact mass along the outer face (the

404   riser) is about 70 m. Assuming the displaced block is a triangular wedge thinning towards

405   the toe (Fig. 4), the volume of the intact slip is ~ 68,250 m^3. Below the main slip there is an

406   area of disintegrated rubble which could increase the length of the riser, potentially adding ~

407   3 % (~ 2300 m^3) to our volume estimate (Table S1 Supplementary Materials). The value of

408   H/L is sometimes considered a mobility ratio, whereby large values of L for relatively small

409   vertical displacement (H) can indicate unimpeded rapid descent and a long runout. Given

410   the volume of the RSF, values of $H/L > 0.6$, as here, indicate no excessive runout (Whittall *et*

411   *al.*, 2017; Table S1 Supplementary Materials).

412

413   The slope of the riser of the RSF mass is currently ~ 30°, that is, is similar to the static angle

414   of repose. This angle may suggest slow downslope movement rather than rapid failure,

415   which tends to produce slope angles much less than the angle of repose. In addition, there

416   was no evidence of hard-rock end-point control at the toe of the slumping block to impede

417   its descent although the toe has rotated outwards (Fig. 4A). The slope of the riser today is

418   less than the slope of the failure plane (44°), which suggests a portion of the intact wedge

419   may be lying above debris derived by over-running some of the disintegrated thin toe of the

420   wedge (Fig. 4A). It is significant that the stratigraphic layers within the main RSF wedge

421   remain intact, with no evident down-slope dilation and little deformation or fracture across

422   the face of the slipped mass. The apparent plunge of the strata (8 to 10° towards the north),

423   *i.e.,* across the face of the RSF, indicates that the western margin of the slip may have

424   descended slightly further downslope than the eastern margin, as the headwall strata plunge

425   6° to 8° in the same direction. The outer face (Fig. 4B) of the RSF has undergone no evident

426   modification.

427

428

429   As shown in Figure 4B, a distinct fault (BGS, 2008b), normal to the cliff face occurs to the

430   east of the RSF at location X, with undisturbed stratigraphy in the headwall either side.

431   Slickenside structures occur along the basal failure plane (c) that continues across the cliff to

432   the north-west. The fault X is aligned with the south-eastern margin of the RSF (as seen in

433   Fig. 4B), whilst a further fault is evident as a distinct fissure in the RSF, with another fault to

434   the north-west (Y). The easterly dip of these three faults could not be determined accurately

435   although they are steep, consistent with the findings of Moseley (1968; 1972) for the

436   Coniston group in the region (see section 5.3). The basal failure plane defined the back of

437   the RSF, whilst the lateral limits to the RSF model were defined by the two marginal fault

438   lines (X,Y).

439

440   **5.2   Estimation of original angle of the outer slope of the rock surface before failure**

441   To apply the *Swedge* model it is necessary to know the angle of the outer slope of the rock

442   face before failure. From the geometry of the residual RSF mass, with respect to the

443   observed failure plane (Fig. 4B), the RSF can be considered as a translational, plane failure of

444   a pentahedron wedge. Taking a side view, the geometry is triangular (Fig. 4B), so it is

445   possible to calculate the minimum slope of the outer rock face prior to slope failure by

446   repositioning the failed block further up the failure plane. The angle of the failure plane is

447   taken as equal to that of the minimum angle of the slickenside surfaces, 44°, with a bearing

448   of between 6 and 11°. The riser (outer face) of the RSF is 70 m in length and the tread width

449   is 15 m; both lengths could have been slightly larger before fracturing occurred along the

450   basal failure plane and at the toe of the RSF (Fig. 4A). Given the small degree of uncertainty

451   with regard to the configuration of the slope before failure, the length of the failure plane

452   (necessarily longer than the riser of the RSF) was varied systematically at the same time as

453   varying the length of the riser between the measured length of 70 m and 90 m; the latter

454   value includes the small area of disintegrated toe (Fig. 4A). The tread width also is varied

455   between the measured breadth of 15 m and a 'limit' of 20 m to allow for potential

456   disintegration along the failure plane at the back of the tread. Repositioning the RSF upslope

457   in this manner, the slope of the outer face could have been no lower than 53° and if the

458   angle of the failure plane is increased beyond ~ 54°, the resulting lengths of the failure plane

459   and outer face become incompatible with field observations.

460

461   **5.3   The Swedge model of the rock slope failure without ice buttressing**

462   Initial application of the Swedge Model used the field data shown in Table 2. We did not

463   model the stability of the wedge in its present position because the basal friction properties

464   are unknown; whether the toe of the RSF rests on rubble derived from the failure plane, or a

465   bedrock surface cannot be determined. Given that the present angle of the riser is 30° and

466   the basal failure plane is at an angle of 44° it is assumed that the wedge is now stable (F>>1).

467

468   The slope of the riser utilized is that applicable to the rock mass before failure, as

469   determined in the preceding section. The width of the tread and the lateral extent (breadth)

470   of the failed mass are determined from the field data. The summit of the cirque is fairly flat

471   so an outward slope of 1° below horizontal is used for the tread; the model is not sensitive

472   to this parameter. The angle of the failure plane is the minimum value for the slickensides to

473   the south-east of the RSF (which were not disturbed by the slope failure). The model allows

474   for defining the additional effective roughness angle (*r*) on the failure planes by applying a

475   'waviness' parameter (*w*) that was determined from the range of recorded slickenside

476   values, following Miller (1988). Other parameters were defined from the field data. It was

477   noted above that the dip of the two lateral delimiting faults could not be determined in the

478   field. However, as local faults tend to be steep (Moseley, 1968; 1972) the model was

479   implemented with the values shown in Table 2 and then varied systematically as reported

480   below. Given the geometry of the problem only three modelling scenarios are necessary to

481   explore the uncertainty in a controlled setting:

482

483   *Model 1: the RSF slides over the basal plane and against Fault Y*. The model aligns

484   the compass orientation of the basal failure plane with the orientation of the riser

485   outer face, which assumes a simple downslope slide. The orientation of Faults X and

486   Y with respect to north are as determined from field data. The X and Y fault dips are

487   steep and both dip to the west. Dips and riser length were varied slightly to optimize

488   the failed volume of the RSF to match the field estimate. In this manner, the model is

489   not consistent with the eastern side of the slip having progressed less far down the

490   failure surface than the western side. Factor of Safety: 0.83.

491

492   *Model 2: the RSF slides along the basal plane and against Fault X*. The model aligns

493   the bearing of the failure plane with the bearing of the slickensides to the east of the

494   RSF, as these define the bearing of the basal failure plane that differs from the

495   bearing of the riser face by 13°. The bearings of Faults X and Y are as determined

496   from field data. The fault dips are steep and both dip to the east. Dips and riser

497   length were varied slightly to optimize the failed volume of the RSF to match the field

498   estimate. In this manner the model is consistent with the eastern side of the slip

499   having progressed less far down the failure surface than the western side. Factor of

500   Safety: 0.86.

501

502   *Model 3: explores the addition of a tension crack to the back of the RSF.* It is not

503   known if a tension crack developed in the actual rock mass before failure, and the

504   properties of the tension crack are determined by the other model attribute values.

505   Including a tension crack, the western side of the RSF extends further down slope

506   than the eastern side, with the lower edge of the model block having a plunge of ~

507   10°, equal to the plunge of the RSF strata in the field. The bearing of the basal failure

508   plane is varied between 6° and 14°. Fault dips are steep, 90° and 62° to the east.

509   Dips and riser length were varied slightly to optimize the failed volume of the RSF to

510   match the field estimate. Given this scenario the RSF slides over the basal plane and

511   against Fault Y. Factor of Safety: 0.52 to 0.83 depending on basal plane bearing.

512

513 Given that there is unavoidable parameter uncertainty, none of the above models is an exact

514 representation of the RSF, although Model 3 is the closest match (Fig. 5). Yet, it is evident

515 that preserving the dip of the basal plane and solving to retain the mass of the failure, any

516 reasonable combination of data leads to a model of the failed block that resembles that seen

517 in nature and, in each case, the Factor of Safety is less than unity. A sensitivity analysis

518 showed that, for reasonable ranges of parameter values (typically ± 10°; outwith those listed

519 in Table 2), usually the geometry of the potential failure did not match that observed and so

520 could be dismissed. Specifically, in the 10,000 simulations of each model, model parameters

521 could be varied (*e.g.,* by ± 5° in the case of angles), retaining a probability of slope failure of

522 96 %. In most cases the factor of safety was between 0.74 and 0.94, and higher factors of

523 safety could not be produced without significant distortion the geometry of the RSF. In a

524 very few cases of parameter combinations (4 %), a marginal factor of safety of between 1.07

525 and 1.22 is achieved. In the latter cases, wetting between 20 and 30 % of the fault planes

526 surface areas, due to percolation of meltwater affecting the water pressure, caused the

527 slope to fail.

528
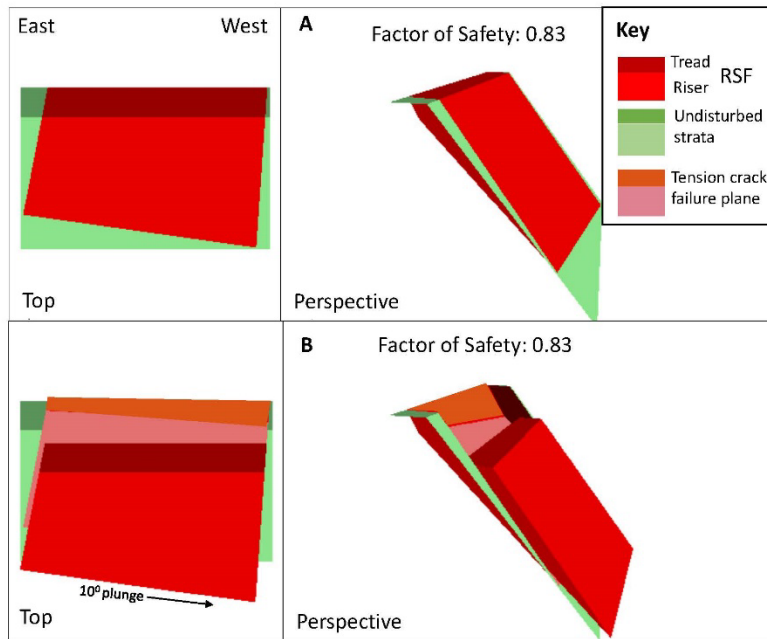
Figure 5: Illustration of Swedge 6.0 Model 3: (A) before failure, and (B) during failure. The basal failure plane orientation is 14° such that the base of the RSF is plunging 10° to the north (right).

As a final consideration it should be noted that in deglaciating mountain regions, RSFs have been related to permafrost degradation and consequent destabilization of ice-filled fractures within the rock mass (Gruber *et al.,* 2004; Gruber and Haeberli, 2007). In the RSF failure model described above, freezing of the failure planes can be considered by simply increasing the friction factors, which can result in the block remaining intact despite the absence of glacial ice buttressing. However, we expect that frozen failure planes did not persist long after glacial down-wasting. Hydrostatic pressure in the failure planes would have been high, and percolation more generally lubricates failure planes (Hasler *et al.,* 2011). In addition, permafrost support for the RSF does not explain the intact stratification of the RSF, as permafrost degradation would have resulted in a rapid RSF. Consequently, permafrost was not considered in any quantitative sense.

5.4   The Swedge model of the rock slope failure with ice buttressing

For the range of simulations reported in the previous section, F < 1 in all the 94 % of physically plausible cases and wetting failure planes resulted in a 100 % failure in all 30,000 cases. Hence, the role of ice buttressing of the riser must be considered, as this is the most likely explanation for slope stabilization. There is no information on the dynamic behaviour

551   of ice within the cirque. Consequently, selecting Model 3 above, three contrasting scenarios

552   can be envisaged that might stabilize the slope: (a) ice can be a static load variably

553   distributed around the centroid (Fig. 6A) of the riser; (b) ice can be dynamic, moving towards

554   the riser such that the stress is variably distributed around the centroid of the riser (Fig. 6B);

555   (c) ice can be dynamic, moving away from the riser such that a bergschrund opens between

556   the ice and the slope and the stress is distributed below the centroid of the riser. Broadly

557   consistent results also are found considering Models 1 and 2 (not reported herein).

558

559   Firstly, considering scenario (a), the weight of an ice load is calculated, and the stress is

560   applied evenly across the area of the riser normal (*i.e.,* 90º) to the slope until it is stabilized

561   (for which condition: F = 1.0065; Fig. 6A). Subsequently, considering scenario (ii), the

562   analysis is repeated to ascertain the optimal direction to apply force that minimizes the ice

563   load. In scenario ii, the ice load can be reduced from that in (a) if the force is directed into

564   the slope and slightly upwards by 13^0 above the horizontal such that for F = 1.0485 (Fig. 6B).

565   In scenario (a), application of 40,659 tonnes of ice is required for a stable slope, which is

566   equivalent to 48,987 m^3, based on a debris-free low ice-density of 830 kg m^{-3} (Colgan and

567   Arenson, 2013). In scenario (b), application of 24,325 tonnes of ice (29,307 m^3) is required

568   for a stable slope. For scenario (c), with a tension crack, the slope will remain stable as long

569   as the total stress applied to the slope is the same as for scenarios (a) or (b). In this study we

570   do not explore in detail how the ice mass and force direction might be distributed across the

571   riser to maintain slope stability as there are multiple permutations. Nonetheless, if the

572   cirque had been filled with ice to the top of the riser, around 166,000 m^3 of ice would be

573   required to fill the volume immediately adjacent to the potential RSF (Fig. 7), which is not

574   compatible with the small ice masses in scenarios (a) and (b) that are required to maintain

575   slope stability. Considering Fig. 7, it is important to recognize that, in any permutation of

576   potential RSF geometry (Table 2), the ice cover required to maintain slope stability is

577   typically less than 29 % (and possible as low as 17 %) of the volume to the top of the riser.

578   This result indicates that the slope would have remained stable as long as there was a

579   sufficiently small degree of ice buttressing due to ice in the cirque contributing a stress

580   normal to the face of the riser—which further implies failure occurred during final

581   deglaciation of the cirque. Note that, although the presence of sufficient ice on the riser

582   alone maintains rock mass stability, it is unlikely that this condition would pertain without

583 ice present immediately adjacent to the rock wedge. So, Figure 7 shows cirque ice beyond

584 the unstable slope, but only conceptually.

585

586
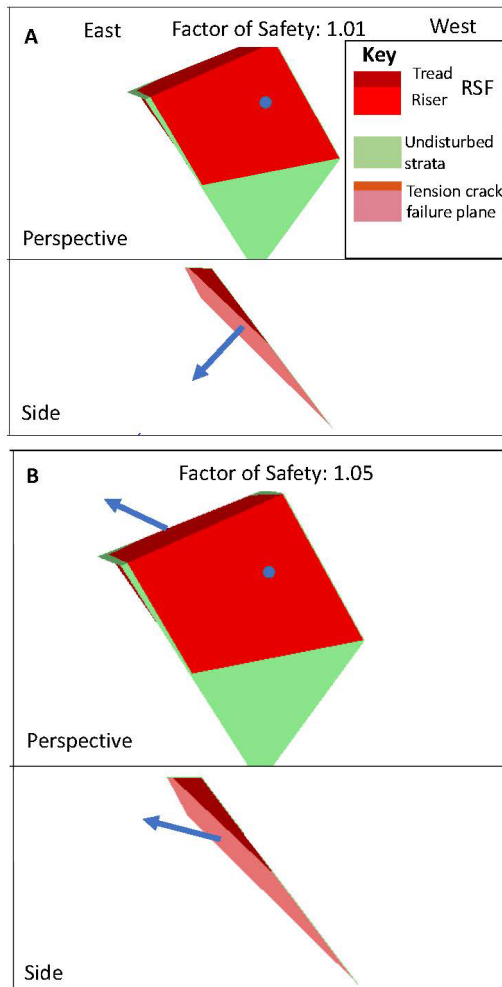
587

588 Figure 6: Illustration of the force application required to stabilize the potential RSF: (A) With
589 the force (point and arrow) applied 90º to the slope, the ice load required to stabilize the
590 slope (i.e., F = 1.0055) is 40,967 tonnes; (B) With the force (point and arrow) applied at the
591 optimum angle (13º above horizontal) the ice load required to stabilize the slope (i.e., F =
592 1.0485) is 28,253 tonnes.
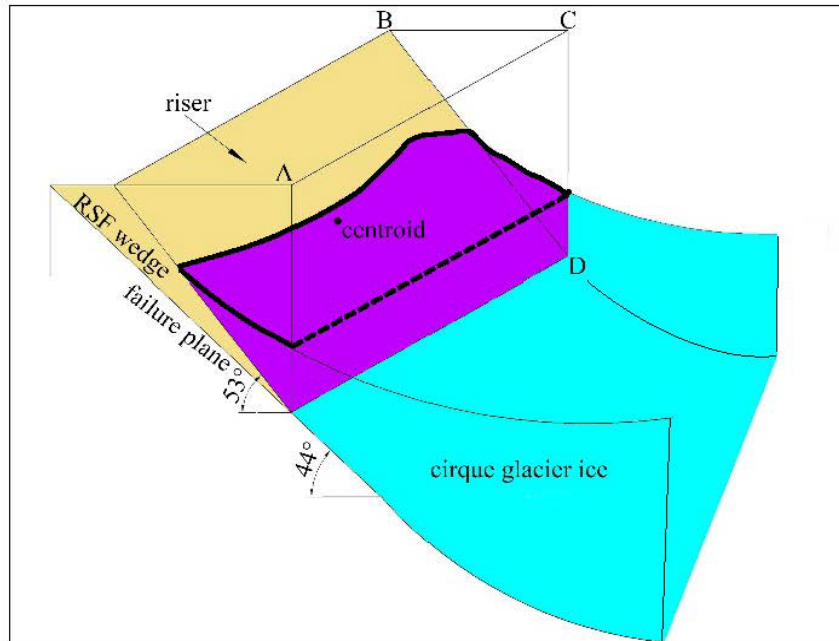
593

594 Figure 7: Cartoon depicting the concept of ice buttressing of the potential RSF. The RSF
595 wedge defines the unstable portion of the slope before the rock slope failure. Points A, B, C
596 and D define a potential pentahedral volume that, if filled by ice, would cover the complete
597 face of the riser. A smaller 'pentahedral' volume (purple), with the upper ice surface
598 outlined by a heavy black line, shows that only a small percentage of the potential
599 pentahedral ice volume is required to be ice-filled to provide buttressing sufficient to
600 prevent slope failure. The inner edge of this pentahedral is show as irregular to indicate
601 potential variable ice loading across the riser. Percentages were obtained from the ice
602 volumes required to buttress the slope. Additional ice might be present in the cirque
603 outside of the defined volume, but this ice does not contribute to the stabilizing load
604 directly applied to the riser.

605

606 **5.5   Exposure ages from the rock slope failure**

607 In both cirques, tills are composed of local lithologies exclusively, and a search for northern-

608 derived erratics confirmed their absence. The absence of erratic lithologies indicates that

609 the cirques were probably finally eroded by locally generated ice masses after the LGM. At

610 the time of the LGM, it is thought that the locations of the cirques were overridden by an ice

611 sheet from the north moving into the northern end of the Lune gorge (Carling *et al.*, 2023).

612 Under such thick ice conditions, the back wall of the cirque would have been stable as the

613 volume of ice was much greater than that required for slope stability—shown by either ice-

614 loading Model 3 scenario a or b. After the LGM, the ice volume in the cirque would

615 decrease such that ice-loading also decreased such that the RSF slowly descended as the

616 loading fell below a critical F-value to sustain the slope. It is this lowering of the RSF that we

617 have attempted to date with cosmogenic nuclides.

618

619 The surface exposure age of 18.0 ± 1.2 ka (sample OSF) postdates the timing of maximum ice

620 cover and is consistent with the timing of deglaciation within the broader region (Carling *et*

621 *al*., 2023) as is considered in the Discussion. As was noted in section 4.2, the outer face of

622 the RSF (the riser) constitutes a smooth surface of intact, undeformed strata, so

623 concordance of the surface exposure age and regional dates is to be expected. Exposure of

624 the RSF riser (sample OSF) predates significantly the exposure age of 12.0 ± 0.8 ka (sample

625 HW) calculated for the RSF basal plane, suggesting a relationship between debuttressing of

626 the riser face and the gradual downward slip of the RSF. The younger age for sample HW is

627 expected, due to the basal failure plane being progressively exposed after the upper portion

628 of the RSF (where sample OSF occurs) was clear of ice cover and the RSF began to move

629 downslope. Also of significance is the fact than the basal failure plane was disrupted by the

630 failure and is friable, as was noted in section 4.2. The loss of only one or two small blocks

631 from the location sampled on the failure plane at any time after failure should result in an

632 age younger than that of the outer face of the RSF (see Supplementary material). Results of

633 the cosmogenic nuclide analyses are summarised in Table 1.

634

635

636 **6.0   Discussion**

637 **6.1 Modelling the RSF dynamics**

638 The *Swedge* model was applied to the RSF assuming the original slope of the rock face was

639 53°, with a slide plane angle of 44° and no ice buttressing. The steeper slickenside surfaces

640 observed in the field directly above the RSF could indicate a steeper failure plane than that

641 used in the model, but these values were not used as they may represent strata disturbed by

642 the RSF. In any case, an increase in the failure plane angle, or the initial angle of the rock

643 face, both increase the propensity for failure. The waviness number calculated from field

644 data and applied in the model is low, which increases the propensity for failure. Preliminary

645 trials showed that to stabilize unstable model slopes would require the use of unrealistically

646 large waviness numbers (Miller, 1988) and so the waviness number was not varied in

647 sensitivity analyses. Thus, our results obtained with the *Swedge* model are conservative but

648   show that the rock face was consistently unstable before failure. The sensitivity analyses

649   accounted for parameter uncertainty and demonstrated that, in most cases, failure would

650   have occurred due to gravity alone. In those few cases where the slope was modelled as

651   marginally stable, moderate water lubrication of the failure surfaces (typically 30% of

652   surfaces) induced slope failure, but the addition of a modest amount of buttressing ice

653   ensured the slope remained stable. As there is no rock obstacle at the toe of the RSF to

654   impede descent, it is reasonable to assume that the slip occurred slowly as the ice decayed.

655   The need for buttressing of the slope to prevent rapid failure indicates that ice support was

656   important (Hilger *et al*., 2018). Thus, our hypothesis '*a steep, faulted, and unstable rock*

657   *slope has experienced buttressing by glacial ice*' as proposed in the Introduction is

658   corroborated here.

659

660   As the amount of Model 3 scenario (a) ice (static load normal to the face) in the cirque

661   decreases, the level of the ice against the riser will fall towards the toe. Thus, the focal point

662   of the force applied to the slope by the ice cover migrates down the riser. As long as the

663   stabilizing load and the direction of the applied force remain sufficient as ice retreats, the

664   detached block will remain stable. However, the load within the cirque is unlikely to be

665   maintained as the ice elevation falls. The applied force also is variable through time and

666   across the riser as ice primarily deforms by internal flow (Hutter, 1983) such that, if any

667   additional pressure were exerted by residual ice adjacent within the Lune gorge, then the ice

668   mass within the cirque would respond accordingly. In particular, the uniaxial compressive

669   strength of ice is low and decreases as ice temperature increases, as will be the case during

670   deglaciation. Although in our model we do not consider the shear stresses associated with

671   the ice in a quantitative sense, brittle fracture of the thin, buttressing ice mass might

672   ultimately occur owing to the constant pressure associated with the mass of the RSF (Bovis,

673   1982; McColl and Davies, 2013). The presence of a tension crack will redistribute ice load

674   and induce ice segregation (frost-cracking) in the rock (Sanders *et al*., 2012) close to the toe

675   of the rock mass, further reducing the competency. So as the factor of safety falls to close to

676   F = 1, the detached block will slowly move downwards. In the final stages of deglaciation,

677   low-density firn (~400–830 kg m^{-3}) will replace glacier ice (~830–917 kg m^{-3}) offering less

678   support to the RSF.

679

680   The RSF failure probably was controlled by distinct intersecting small-scale faults, as has

681   been modelled herein. Within the general area of Great Coum there appears to be two sets

682   of frequent lineaments, one trending to N to NW and the other NE, that intersect to define

683   bedrock blocks. Despite this propensity, the other steep headwalls in these two cirques

684   show no evidence of large-scale instability, although the basal fault plane of the RSF extends

685   (Fig. 4) behind the more western steep buttress in Great Coum, indicating that this slope is

686   also potentially unstable. One fault (BGS, 2008b) and several other lineaments occur roughly

687   normal to this alignment which, in conjunction, might delimit a potential wedge failure on

688   this western buttress. In the specific case modelled, slope failure is highly site-specific

689   depending, in the main, on fault alignments. Steepening of the cirque headwall via glacial

690   erosion may have altered the disposition of the rock mass load, increasing tensile stresses

691   along the fault planes, and promoting the RSF (Ballantyne, 2002). In this respect, the failed

692   slope was pre-conditioned (*sensu* McColl and Davies, 2013) to fail. However, the modelling

693   suggests that unloading likely played a role in controlling the timing of failure and the rate of

694   landslide displacement once initiated. Unloading may simply allow the unsupported

695   preconditioned block to fail, but the stress release accompanying unloading usually is

696   propagated along the fault network resulting in a reduction of internal locking stresses (*i.e.*,

697   the waviness number; Wyrwoll, 1977; Ballantyne, 2002). Other preparatory factors also

698   come into play as the ice load was removed, such as lubrication of the failure planes by

699   meltwater and weathering of the fault planes in general, moving the block closer to F = 1.

700

701   **6.2 Timing of the RSF**

702   Although there is only one terrestrial cosmogenic date for the riser of the RSF, the surface

703   exposure dating of 18ka (sample OSF) is compatible with the RSF movement during final

704   deglaciation around 19.2 to 16.6 ka (see Carling *et al*., 2023, for a review of regional dates).

705   We interpret the much younger exposure age (~ 12 ka) on the fault plane (sample HW) as

706   the result of postglacial weathering and erosion of the fractured failure plane. In contrast,

707   much of the surface of the riser is relatively intact. Exposure dating necessarily only yields a

708   minimum-limiting age of exposure, except in cases where primary structures (*e.g.*, glacial

709   striations or slickensides) testify to negligible surface erosion. We observed some

710   slickensides locally preserved on the fault plane, but some degree of surface erosion is also

711   indicated by a scattering of talus and a shattered basal failure plane. We provide an estimate

712   of the magnitude of surface erosion assuming a range of plausible erosion rates in Fig. S2,

713   Supplementary Materials wherein the limitations of having only two cosmogenic samples is

714   addressed.

715

716   We note that the locally derived till and absence of northern derived erratics in the cirques

717   suggests that northern ES1 ice did not enter the cirques, despite the presence of abundant

718   (northern) Shap granite erratics in Borrowdale, Roundthwaite valley and Bretherdale just to

719   the north (Carling *et al.*, 2023). Thus, buttressing of the slope by ice moving into the cirque

720   from the north can be ruled out. We suggest that the two cirques probably fed valley

721   glaciers associated with diminishing plateau icefields after the LGM (Carling *et al.*, 2023), and

722   their final form evolved during deglaciation. The Devensian termination is thought to be a

723   4–5 kyr period of ice decay just prior to the Last Glacial-Interglacial Transition at ~ 14.7–11.5

724   ka (Stone *et al.*, 2010). During deglaciation, there was unlikely to be sufficient ice in the

725   adjacent Lune gorge to bolster the cirque ice mass.

726

727   Regarding slope failures in cirques, Cave and Ballantyne (2016) and Klimeŝ *et al. (*2021)

728   noted that the role of glacial ice support in cirque back wall stability is conditioned by the

729   associated time scales considered. For example, Klimeŝ *et al. (*2021) reported high factors of

730   safety (> 1.95) for potential RSFs beneath glacial ice during the LGM, which is assumed to be

731   the case during full glacial conditions. Ballantyne *et al.* (2014) demonstrated that, following

732   the LGM, the timing of several dated RSFs is not consistent with the probable timing of

733   glacial debuttressing, reporting ages that correspond to deglaciation and well after. In

734   contrast, at Great Coum, the surface exposure age of 18.0 ± 1.2 ka is consistent with regional

735   estimates of the timing of deglaciation (see Carling *et al.*, 2023), as was noted above.

736   However, the apparent delay in final exposure of the fault plane, sometime before 12.0 ± 0.8

737   ka, indicates that a range of exposure ages might be associated with arrested RSFs; indeed,

738   some post-glacial dates may be associated with isostatic controls on slope failure (Ballantyne

739   et al., 2014).

740

741   **6.3 An ice advance during the Younger Dryas?**

742   An important remaining issue is whether Great Coum could have supported a glacier during

743   the Younger Dryas Stadial. Although the Lake District was essentially ice-free by ~ 14.7 ka,

744   Younger Dryas cooling led to a subset of cirques in northern Britain refilling briefly (Evans,

745   1997). Sissons (1980) argued that many central Lake District cirques were re-occupied by ice

746   during the Younger Dryas, and subsequent studies (reviewed by Brown *et al.*, 2011) indicate

747   the presence of cirque glaciers in the central Lake District. However, the lowest Lake District

748   cirque floors are around 320 m asl (Temple, 1965), whereas the basal lip of Little Coum lies

749   at 262 m asl. In this context, Manley (1961) argued that cirques in the Howgill Fells lack

750   evidence for reoccupation during the Younger Dryas because they are too low. Norris and

751   Evans (2017) suggested the ELA in the western Pennines was 580 m asl during the Younger

752   Dryas with the lowest estimate placing the altitude at 445 m asl (Wilson and Clark, 1995).

753   Similarly, in the eastern Lake District, immediately to the north-west of Great Coum, the ELA

754   has been estimated at 400–600 m with 400 m being regarded as distinctly marginal (Wilson

755   and Clark, 1998). Glacial ice only descended to altitudes below 400 m asl where small outlet

756   glaciers were fed from plateau icefields (McDougall, 2013), the extents of which remain

757   controversial (Bickerdike *et al.*, 2018). In this respect, Harvey (1997) noted that there was

758   no evidence of ice readvance in the west facing Carlingill, neighbouring Great Coum.

759

760   As the top of the headwall of Great Coum is at 468 m asl, with no extensive plateau above, it

761   seems unlikely that snow supply was sufficient to maintain a Younger Dryas cirque glacier.

762   Others have also noted that Howgill cirques are too low to support Younger Dryas ice but

763   have suggested that the 'fresh' appearance of moraines in some Howgill and western

764   Pennine cirques indicate that Younger Dryas ice was maintained locally by extensive snow-

765   blow (Gunson, 1966; Gunson and Mitchell, 1991; Mitchell, 1996). If correct, this would

766   reduce the ELA locally to as low as 311 m asl (Mitchell, 1996). Mitchell's estimate of ELA is

767   similar to the best estimate for Little Coum (300 m asl), and it is noted by several authorities

768   (Manley, 1961; Temple, 1965; Mitchell, 1996) that the dominant wind direction during the

769   Younger Dryas was from the W and SW, associated with cyclonic disturbances.

770   Nevertheless, we are not convinced by this argument. The extensive SW-facing slopes of

771   Grayrigg Forest and Grayrigg Pike are below the Younger Dryas ELA, so it is unlikely that

772   sufficient blown-snow could have been supplied to support glacial ice within the Great and

773   Little Coums. Our exposure age of 18.0 ± 1.2 ka (sample OSF) denoting ice-free conditions

774   on the outer face of the RSF suggests the cessation of glacial erosion at Great Coum.

775

7.0   Conclusions

We have demonstrated that a RSF in the headwall of a cirque in the Lune gorge occurred as a slow downslope movement of an intact rock mass due to the presence of a supporting glacial ice mass buttressing the failed slope. The estimated RSF timing corresponds with regional deglaciation occurring by at least 18.0 ± 1.2 ka.

Although the case study reported herein supports the role of ice buttressing as a process which may explain arrested RSFs, the vagaries of rock structure from one location to another, coupled with the spatially variable role of isostatic uplift and local meltwater climate (Cave and Ballantyne, 2016) provide strong site-specific controls on the nature and timing of RSFs. Further modelling of RSFs should elucidate the range of conditions associated with incipient failure whilst additional exposure ages for rock surfaces should assist in constraining the timing during which processes such as glacial debuttressing applied.

Code availability

Swedge 6.0 is available from Rocscience Inc., Toronto (www.rocscience.com) for purchase or as a licenced educational package upon application.

Supplement Link

Note to reviewer: A supplement accompanies this manuscript

Author Contribution

PAC devised the project and conducted the fieldwork and the *Swedge 6.0* simulations. TS assisted in fieldwork. PAC and JDJ wrote the manuscript. JLA and MFK conducted the cosmogenic nuclide analysis. All authors contributed to the final presentation.

Competing interests

The authors declare that they have no conflict of interest.

Acknowledgements

Teng Su was supported by the State Scholarship Fund of the China Scholarship Council, including a study visit hosted by the Lancaster Environment Centre, Lancaster University. Rocscience Inc., Toronto is thanked for supplying *Swedge 6.0* as an educational package. Wishart Mitchell kindly provided a copy of the Gunson (1966) thesis. Mike Cavanagh and the Horned Beef Company are thanked for access permissions to collect rock samples in the

808   cirque. Sam McColl is thanked for commentary on an early version of the manuscript which

809   contributed to the final presentation. The reviewers, David Jarman and Tim Davies, are

810   thanked for their detailed commentaries on the submission.

811

812   **Data Availability Statement**

813   The data required as input to *Swedge* version 6.0 (2018) are listed in Table 2. Use of *Swedge*

814   version 6.0 was licensed under an educational agreement with Rocscience Ltd., 2018:

815   www.rocscience.com. The [10]Be concentrations and underlying AMS data associated with the

816   [10]Be exposure ages are published on GitHub

817   https://github.com/CosmoAarhus/LakeDistrict_CosmoData.

818

819   **References**

820   Allen, S. K., Cox, S. C., and Owens, I. F., 2010. Rock avalanches and other landslides in the

821   central Southern Alps of New Zealand: a regional study considering possible climate change

822   impacts. *Landslides*, 8, 33-48.

823

824   Andersen, J.L., Egholm, D.L., Knudsen, M.F., Jansen, J.D., Nielsen, S.B., 2015. The periglacial

825   engine of mountain erosion – Part 1: Rates of frost cracking and frost creep. *Earth Surface*

826   *Dynamics*, 3, 447-462.

827

828   Andersen, J. L., Egholm, D. L., Olsen, J., Larsen, N. K., and Knudsen, M. F. (2020).

829   Topographical evolution and glaciation history of South Greenland constrained by paired

830   26Al/10Be nuclides. *Earth and Planetary Science Letters*, 542, 116300.

831

832   Aveline, W.T., Hughes, T.M., Strahan, A. 1888. The Geology of the Country around Kendal,

833   Sedbergh, Bowness and Tebay. Memoirs of the Geological Survey, England and Wales,

834   London, 94pp plus 3 Plates.

835

836   Ballantyne, C.K. 2002. Paraglacial geomorphology. *Quaternary Science Reviews*, 21, 1935–

837   2017.

838

839   Ballantyne, C.K., Periglacial Geomorphology, Wiley, 472pp, 2018.

840

841   Ballantyne, C. K., Wilson, P., Gheorghiu, D. and Rodés, À., 2014. Enhanced rock-slope failure

842   following ice-sheet deglaciation: timing and causes. *Earth Surface Processes and Landforms*,

843   39, 900–913.

844

845   Barr, I.D., Ely, J.C., Spagnolo, M., Clark, C.D., Evans, I.S., Pellicer, X.M., Pellitero, R., Rea, B.R.

846   2017. Climate patterns during former periods of mountain glaciation in Britain and Ireland:

847   Inferences from the cirque record. *Palaeogeography, Palaeoclimatology, Palaeoecology*,

848   485, 466–475.

849

850   BGS (British Geological Survey), http://www.bgs.ac.uk/data/boreholescans/home.html,

851   accessed 2022, undated.

852

853   BGS, 2008a. Geological Survey of England and Wales 1:50,000 geological map series, New

854   Series Sheet 39, Bedrock, Kendal.

855

856   BGS, 2008b. Geological Survey of England and Wales 1:50,000 geological map series, New

857   Series Sheet 39, Bedrock and Superficial Deposits, Kendal.

858

859   Bickerdike, H.L., Ó Cofaigh, C., Evan, D.J.A., Stokes, C.R., 2018. Glacial landsystems, retreat

860   dynamics and controls on Loch Lomond Stadial (Younger Dryas) glaciation in Britain. *Boreas*,

861   47, 202-224.

862

863   Bonilla-Sierra, V., Scholtès, L., Donzé, F.-V., Elmouttie, M. 2015. DEM analysis of rock bridges

864   and the contribution to rock slope stability in the case of translational sliding failures.

865   *International Journal of Rock Mechanics and Mining Sciences*, 80, 67–78.

866

867   Bovis, M.J. 1982. Uphill-facing (antislope) scarps in the Coast Mountains, southwest British

868   Columbia. *Geological Society of America Bulletin*, 93, 804-812.

869

870   Brown, V.H., Evans, D.J.A., Evans, I.S. 2011. The glacial geomorphology and surficial geology

871   of the south-west English Lake District. *Journal of Maps*, 7, 221–243.

872

873   Brown, V. H., Evans, D. J. A., Vieli, A. and Evans, I. S. 2013. The Younger Dryas in the English

874   Lake District: reconciling geomorphological evidence with numerical model outputs. *Boreas*,

875   42, 1022–1042.

876

877   Carling, P.A., Su, T., Meshkova, L., 2023. Distribution of Devensian glacial erratics and related

878   evidence elucidate complex ice flow changes across a former ice divide: Northern England.

879   *Proceedings of the Geologists' Association*, 134, 139-165.

880

881   Cave, J.A.S. and Ballantyne, C.K., 2016. Catastrophic rock-slope failures in NW Scotland:

882   quantitative analysis and implications, Scottish *Geographical Journal*, 132, 185-209.

883

884   Chiverrell , R.C. and Thomas, G.S.P., 2010. Extent and timing of the last glacial maximum

885   (LGM) in Britain and Ireland: a review. *Journal of Quaternary Science*, 25, 535-549.

886

887   Chiverrell, R.C., Smedley, R.K., Small, D., Ballantyne, C.K., Burke, M.J., Callard, S.L., Clark,

888   C.D., Duller, G.A.T., Evans, D.J.A., Fabel, D., Van Landeghem, K., Livingstone, S.,

889   O Cofaigh, C., Thomas, G.S.P., Roberts, D.H., Saher, M., Scourse, J.D., Wilson, P., 2018.

890   Ice margin oscillations during deglaciation of the northern Irish Sea Basin. *Journal*

891   *of Quaternary Science*, https://doi.org/10.1002/jqs.3057 (ISSN 0267-8179).

892

893   Clark, P.U., Dyke, A.S., Shakun, J.D., Carlson, A.E., Clark, J., Wohlfarth, B., Mitrovica, J.X.,

894   Hostetler, S.W., McCabe, M., 2009. The last glacial maximum. *Science*, 325, 710–714.

895

896   Clark, C.D., Ely, J.C., Greenwood, S.L., Hughes, A.L.C., Meehan, R., Barr, I.D., Bateman, M.D.,
897   Bradwell, T., Doole, J., Evans, D.J.A., Jordan, C.J., Monteys, X., Pellicer, X.M. Sheehy, M.,
898   2018. BRITICE Glacial Map, version 2: a map and GIS database of glacial landforms of the last
899   British–Irish Ice Sheet. *Boreas*, 47, 11–27. https://doi.org/10.1111/bor.12273.
900

901   Cody, E., McColl, S., Draebing, D., Cook, S., 2018. Structural control and development of the

902   ice buttressed Mueller rockslide, New Zealand. Geophysical Research Abstract 30, EGU2018-

903   10748, EGU General Assembly 2018.

904

905   Colgan, W., Arenson, L.U., 2013. Open-pit glacier ice excavation: brief review. *Journal of Cold*

906   *Regions Engineering*, 27, 223-243.

907

908   Cossart E, Braucher R, Fort M, Bourlès DL, Carcaillet J. 2008. Slope instability in relation to

909   glacial debuttressing in alpine areas (Upper Durance catchment, southeastern France):

910   Evidence from field data and 10Be cosmic ray exposure ages. *Geomorphology*, 95: 3–26.

911

912   Davies, B.J., Livingstone, S.J., Roberts, D.H., Evans, D.J.A., Gheorghiu, D.M., Ó Cofaigh, C.,

913   2019. Dynamic ice stream retreat in the central sector of the last British-Irish Ice Sheet.

914   *Quaternary Science Reviews*, 225, 105989.

915

916   Ehlers, J., Gibbard, P.L., Overview. In: *Encyclopedia of Quaternary Science, vol. 2.*, Elias, S.A.

917   (ed.), Elsevier, Amsterdam, 143-150, 2013.

918

919   Evans, I.S., Cirques and moraines of the Helvellyn Range, Cumbria: Grisdale and Ullswater, In:

920   Geomorphology of the Lake District: A Field Guide, edited by J. Boardman, BGRG Spring Field

921   Meeting, 16-18 May 1997, BGRG, pp. 63-87, 1997.

922

923   Goodchild, J.G., 1875. The glacial phenomena of the Eden valley and the western part of the

924   Yorkshire Dales District. *Quarterly Journal of the Geological Society*, 31, 55-99.

925

926   Goodchild, J.G., 1889. An outline of the geological history of the Eden valley or Edenside.

927   *Proceedings of the Geological Association*, 2, 258-284.

928

929   Gruber, S., Hoezle, M. and Haeberli, W., 2004. Permafrost thaw and destabilization of Alpine

930   rockwalls in the hot summer of 2003. *Geophysical Research Letters*, 31, L13504.

931

932   Gruber, S. and Haeberli, W., 2007. Permafrost in steep bedrock slopes and its temperature-
933   related destabilization following climate change. *Journal of Geophysical Research*, 112,
934   F02S18.

935

936   Gunson, A.R., Some aspects of the Lateglacial Period in the Western Pennines area.
937   Unpublished M.A. thesis, University of Lancaster, 134pp, 1966.

938

939   Gunson, A.R., Mitchell, W.A., Combe Scar, In: Western Pennines: Field Guide, W.A. Mitchell
940   (ed.), Quaternary Research Association, London, pp 104- 110, 1991.

941

942   Harkness, R., 1870. On the distribution of Wastdale-Crag blocks, "Shap-granite boulders" in
943   Westmorland. *Quarterly Journal of the Geological Society*, 26, 517-528.

944

945   Harley, J.B., 1975. Chapter 11 The accuracy of Ordnance Survey maps, In: Ordnance Survey
946   Maps a descriptive manual, HMSO, London.

947

948   Hartmeyer, I., Delleske, R., Keuschnig, M., Krautblatter, M., Lang, A., Schrott, L., Otto, J.-C.,
949   2020. Current glacier recession causes significant rockfall increase: The immediate
950   paraglacial response of deglaciating cirque walls. *Earth Surface Dynamics: Discussions*,
951   https://doi.org/10.5194/esurf-2020-8

952

953   Harvey A.M., Fluvial geomorphology of north-west England. In: Gregory K.J. (ed) Fluvial
954   Geomorphology of Great Britain. The Geological Conservation Review Series. Springer,
955   Dordrecht, 173-200, 1997.

956

957   Hasler, A., Gruber, S., Font, M. and Dubois, A., 2011. Advective heat transport in frozen rock
958   clefts: conceptual model, laboratory experiments and numerical simulation. *Permafrost and*
959   *Periglacial Processes*, 22, 378–389.

960

961   Hilger,P., Hermanns, R.L., Gosse, J.C., Jacobs, B., Etzelmüller, B., Krautblatter, M., 2018.
962   Multiple rock-slope failures from Mannen in Romsdal Valley, western Norway, revealed from
963   Quaternary geological mapping and 10Be exposure dating. *The Holocene*, 28, 1841–1854.

964

965 Hoek, E.T., Bray, J.W., Rock Slope Engineering. 3rd ed. Institute of Mining and Metallurgy,

966 London, 1981.

967

968 Hollingsworth, S.E. 1931. Glaciation of western Edenside and the adjoining areas and the

969 drumlins of Edenside and the Solway plain. *Quarterly Journal of the Geological Society*, 87,

970 281-357.

971

972 Holm, K., Bovis, M., and Jakob, M., 2004. The landslide response of alpine basins to post-

973 Little Ice Age glacial 520 thinning and retreat in southwestern British Columbia,

974 *Geomorphology*, 57, 201-216.

975

976 Hutter, K., Theoretical Glaciology: Material Science of Ice and the Mechanics of Glaciers and

977 Ice Sheets, Springer, 1983.

978

979 Jarman, D., 2005. Large rock slope failures in the Highlands of Scotland: Characterisation,

980 causes and spatial distribution. *Engineering Geology*, 83, 161-182.

981

982 Jarman, D., Wilson, P., Clough Head - Threlkeld Knotts: A perplexing RSF complex. In: The

983 Quaternary of the Lake District - Field Guide, McDougall, D.A. and Evans, D.J.A. (eds)

984 Quaternary Research Association, London, 153–173, 2015a.

985

986 Jarman, D., Wilson, P. 2015b. Anomalous terrain at Dove Crags 'cirqueform' and Gasgale Gill

987 asymmetric valley, English Lake District, attributed to large-scale rock slope failure of pre-

988 LGM origins. *Proceedings of the Yorkshire Geological Society*, 60, 243–257.

989

990 Jaeger, J.C., Cook, N.G.W., Fundamentals of Rock Mechanics, 3rd edn. Chapman and Hall,

991 London, 1979.

992

993 Klimeŝ, J., Novotný, J., Rapre, A.C., Balek, J., Pavel Zahradníĉek, J.C., Strozzi, T., Sana, H., Frey,

994 H., René, M., Štěpánek, P., Meitner, J., Junghardt, J., 2021. Paraglacial rock slope stability

995   under changing environmental conditions, Safuna Lakes, Cordillera Blanca Peru. *Frontiers in*

996   *Earth Science*, 9: 607277. doi: 10.3389/feart.2021.607277

997

998   Lal, D. 1991., Cosmic-ray labeling of erosion surfaces: in situ nuclide production rates and

999   erosion models. *Earth and Planetary Science Letters*, 104, 424-439.

1000

1001   Le Roux, O., Schwartz, S., Gamond, J.F., Jongmans, D., Bourles, D., Braucher, R., Mahaney,

1002   W., Carcaillet, J., Leanni, L., 2009. CRE dating on the head scarp of a major landslide

1003   (Séchilienne, French Alps), age constraints on Holocene kinematics. *Earth and Planetary*

1004   *Science Letters*, 280: 236–245. https://doi.org/10.1016/j.epsl.2009.01.034

1005

1006   Letzer, J.M., The glacial geomorphology of the region bounded by Shap Fells, Stainmore and

1007   the Howgill Fells in east Cumbria. Unpublished M.Phil. thesis, University of London, 340pp,

1008   1978.

1009

1010   Lifton, N., Sato, T., and Dunai, T. J. (2014). Scaling in situ cosmogenic nuclide production

1011   rates using analytical approximations to atmospheric cosmic-ray fluxes. *Earth and Planetary*

1012   *Science Letters*, *386*, 149-160.

1013

1014   Livingstone, S.J., Evans, D.J.A., Ó Cofaigh, C., 2010. Re-advance of Scottish ice into the Solway

1015   Lowlands (Cumbria, UK) during the Main Late Devensian deglaciation. *Quaternary Science*

1016   *Reviews*, 29, 2544-2570.

1017

1018   Livingstone, S.J., Evans, D.J.A., Cofaigh, C. Ó, Davies, B.J., Merritt, J.W., Huddart, D., Mitchell,

1019   W.A., Roberts, D.H., Yorke, L., 2012. Glaciodynamics of the central sector of the last British-

1020   Irish Ice Sheet in Northern England. *Earth-Science Reviews*, 111, 25–55.

1021

1022   Lowe, J.J., Rasmussen, S.O., Björck, S., Hoek, W.Z., Steffensen, J.P., Walker, M.J.C., Yu, Z.C.

1023   and the INTIMATE group. 2008. Synchronisation of palaeoenvironmental events in the North

1024   Atlantic region during the Last Termination: a revised protocol recommended by the

1025   INTIMATE group. *Quaternary Science Reviews* 27, 6-17.

1026

1027   Manley, G., 1961. The Late-glacial climate of North-West England. *Geological Journal*, 2, 188-
1028   215.

1029

1030   Marr, J.E., Fearnsides, W.G., 1909. The Howgill Fells and their topography. *Quarterly Journal*
1031   *of the Geological Society*, 65, 587- 610 plus plates.

1032

1033   McColl, S.T. 2012. Paraglacial rock-slope stability. *Geomorphology*, 153-154, 1-16.

1034

1035   McColl, S.T., Davies, T.R.H., McSaveney, M.J. 2010. Glacier retreat and rock-slope stability:
1036   debunking debuttressing. Delegate Papers, Geologically Active, 11th Congress of the
1037   International Association for Engineering Geology and the Environment, Auckland, Aotearoa,
1038   5-10 September 2010, Auckland, New Zealand, 467-474.

1039

1040   McColl, S.T., Davies, T.R.H. 2013. Large ice-contact slope movements: glacial buttressing,
1041   deformation and erosion. *Earth Surface Processes and Landforms*, 38, 1102-1115.

1042

1043   McDougall, D., 2013. Glaciation style and the geomorphological record: evidence for
1044   Younger Dryas glaciers in the eastern Lake District, northwest England. *Quaternary Science*
1045   *Reviews*, 73, 48-58.

1046

1047   Merritt, J.W., Hall, A.M., Gordon, J.E., Connell, E.R., 2019. Late Pleistocene sediments,
1048   landforms and events in Scotland: a review of the terrestrial stratigraphic record. *Earth and*
1049   *Environmental Science Transactions of the Royal Society of Edinburgh,* 110, 39–91.

1050

1051   Miller, S.M., Modelling shear strength at low normal stresses for enhanced rock slope
1052   engineering, In: *Proceedings of the 39th Highway Geology Symposium,* Park City, Utah,
1053   August 17-19, pp 346-356, 1988.

1054

1055   Mitchell, W. A., 1996. Significance of snowblow in the generation of Loch Lomond Stadial
1056   (Younger Dryas) glaciers in the western Pennines, northern England. *Journal of Quaternary*
1057   *Science,* 11**,** 233 - 248.

1058

1059   Moore, J. R., Sanders, J. W., Dietrich, W. E., and Glaser, S. D., 2009. Influence of rock mass

1060   strength on the erosion rate of alpine cliffs. *Earth Surface Processes and Landforms,* 34,

1061   1339-1352.

1062

1063   Moseley, F., 1968. Joints and other structures in the Silurian rocks of the southern Shap Fells,

1064   Westmorland. *Geological Journal*, 6, 79-96.

1065

1066   Moseley F., 1972. A tectonic history of N.W. England. *Quarterly Journal of the Geological*

1067   *Society of London*, 128, 561-598.

1068

1069   Moulson, J.R., Some Aspects of the Geomorphology of the Lune Basin. Unpublished M.A.

1070   thesis, University of Manchester, 1966.

1071

1072   Norris, S.L., Evans, D.J.A., High Cup Plain – a Younger Dryas palaeoglacier. In: Evans D.J.A.

1073   (ed.), The Quaternary Landscape History of Teesdale and the North Pennines – Field Guide.

1074   Quaternary Research Association, London, pp. 231-236, 2017.

1075

1076   Porter, S.C. 2001. Snowline depression in the tropics during the Last Glaciation. *Quaternary*

1077   *Science Reviews*, 20, 1067-1091.

1078

1079   Rasmussen, S. O., Andersen, K. K., Svensson, A. M., Steffensen, J. P., Vinther, B. M., Clausen,

1080   H. B., Siggaard-Andersen, M.-L.; Johnsen, S. J., Larsen, L. B.; Dahl-Jensen, D., Bigler, M.,

1081   2006. A new Greenland ice core chronology for the last glacial termination. *Journal of*

1082   *Geophysical Research*, 111 (D6): D06102.

1083

1084   Rocscience Ltd., SWEDGE-Probabilistic analysis of the geometry and stability of surface

1085   wedges. Toronto, Canada; www.rocscience.com, 2018.

1086

1087   Rose, J., Letzer, J.M., 1977. Superimposed drumlins. *Journal of Glaciology*, 18, 471-480.

1088

1089   Rose, J., 1985. The Dimlington Stadial/Dimlington Chronozone: a proposal for naming the

1090   main glacial episode of the Late Devensian in Britain. *Boreas* 14, 225-230.

1091

1092   Sanders, J.W., Cuffey, K.M., Moore, J.R., MacGregor, K.R., Kavanaugh, J.L., 2012. Periglacial

1093   weathering and headwall erosion in cirque glacier bergschrunds. *Geology*, 40, 779-782.

1094

1095   Sass, O., 2005. Spatial patterns of rockfall intensity in the northern Alps. *Zeitschrift für*

1096   *Geomorphologie*, 138, 51-65.

1097

1098   Scourse, J.D., Haapaniemi, A.I., Colmenero-Hidalgo, E., Peck, V.L., Hall, I.R., Austin, W.E.N.,

1099   Knutz, P.C. and Zahn, R., 2009. Growth, dynamics and deglaciation of the last British-Irish ice

1100   sheet: the deep-sea ice-rafted detritus record. *Quaternary Science Reviews*, 28, 3066-3084.

1101

1102   Sissons, J.B., 1980. The Loch Lomond Advance in the Lake District, northern England.

1103   *Transactions of the Royal Society of Edinburgh: Earth Sciences*, 71, 13-27.

1104

1105   Soper, N.J., The Windermere Supergroup of 1:25,000 sheets NY50 and NY60. Southern Shap

1106   Fells and Northern Howgill Fells, Cumbria. British Geological Survey Technical Report

1107   WA/99/35. 18pp plus 8 figures, 1999.

1108

1109   Soper, N J., Notes on the Windermere supergroup of the country between Kendal and the

1110   River Lune (1: 25 000-scale sheets SD59 and SD69 west). British Geological Survey Internal

1111   Report, IR/06/081. 15pp, 2006.

1112

1113   Stead, D., Wolter, A., 2015. A critical review of rock slope failure mechanisms: the

1114   importance of structural geology. *Journal of Structural Geology*, 74, 1-23.

1115

1116   Stone, P., Millward, D., Young, B., Merritt, J. W., Clarke, S. M., McCormac, M., Lawrence, D. J.

1117   D., Main Late Devensian glaciation of north-west England, In: British Regional Geology:

1118   Northern England. Fifth edition. British Geological Survey, Keyworth, Nottingham,

1119   http://earthwise.bgs.ac.uk/index.php/British regional geology: Northern England, 2010.

1120

1121   Taylor, B.J., Burgess, I.C., Land, D.H., Mills, D.A.C., Smith, D.B., Warren, P.T., Northern

1122   England: British Regional Geology, Fourth Edition, London, HMSO, 125pp, 1971.

Temple, P.H., 1965. Some aspects of cirque distribution in the west-central Lake District, northern England. *Geografiska Annaler*, 47A, 185-193.

Whalley, W. B., Douglas, G. R., Jonnson, A., 1983. The magnitude and frequency of large rockslides in Iceland in the postglacial. *Geografiska Annaler*, 65A, 99–110.

Whittall, J., Eberhardt, E., McDougall, S., 2017. Runout analysis and mobility observations for large open pit slope failures. *Canadian Geotechnical Journal*, 54, 373-291.

Wilson, P. 2005. Paraglacial rock-slope failures in Wasdale, western Lake District, England: morphology, styles and significance. *Proceedings of the Geologists' Association*, 116, 349–361.

Wilson, P., Clark, R. 1995. Landforms associated with a Loch Lomond Stadial glacier at Cronkley Scar, Teesdale, northern Pennines. *Proceedings of the Yorkshire Geological Society*, 50, 277-283.

Wilson, P., Clark, R., 1998. Characteristics and implications of some Loch Lomond Stadial moraine ridges and later landforms, eastern Lake District, northern England. *Geological Journal*, 33, 73-87.Wilson, P., Clark, R. and Smith, A. 2004. Rock-slope failures in the Lake District: A preliminary report. *Proceedings of the Cumberland Geological Society*, 7, 13–36.

Wilson, P., Lord, T., 2014. Towards a robust deglacial chronology for the northwest England sector of the last British-Irish Ice Sheet, *North West Geography*, 14, 1-11.

Wilson, P., Jarman, D., 2022. Rock slope failure in the Lake District, NW England: an overview, *Geografiska Annaler: Series A, Physical Geography*, 104:3, 201-225, DOI: 10.1080/04353676.2022.2120261

Wyrwoll, K-H., 1977. Causes of rock-slope failure in a cold area: Labrador-Ungava. *Geological Society of America Reviews in Engineering Geology*, 3, 59–67.